Chemical Engineering Journal Advances 12 (2022) 100385

Contents lists available at ScienceDirect

Chemical Engineering Journal Advances

journal homepage: www.sciencedirect.com/journal/chemical-engineering-journal-advances

Deep aerobic desulfurization of fuels over iron–containing zeolite based catalysts

Argam V. Akopyan [a,*], Ekaterina A. Eseva [a], Dmitriy E. Tsaplin [a], Sofya Sh. Latypova [a], Daria A. Makeeva [a], Alexander V. Anisimov [a], Anton L. Maximov [a,b], Eduard A. Karakhanov [a]

[a] Chemistry Department, Lomonosov Moscow State University, Leninskie gory, 1/3, 119234 Moscow, Russia
[b] A.V. Topchiev Institute of Petrochemical Synthesis, 29 Leninsky prospect, 119991 Moscow, Russia

ARTICLE INFO

Keywords:
Aerobic oxidative desulfurization
Dibenzothiophene
Iron-containing zeolite-based catalyst
ZSM-12
ZSM-5

ABSTRACT

Herein, we present a new approach to the design of the catalysts for aerobic oxidation of sulfur-containing compounds. Iron-containing zeolite-based (ZSM-5, ZSM-12) catalysts were synthesized and successfully tested in oxidation of model mixtures as well as real petroleum fractions. The catalysts were characterized by means of X-ray diffraction (XRD), X-ray fluorescence spectroscopy (XRF), scanning electron microscopy (SEM), ultraviolet–visible spectroscopy (UV/Vis), temperature programmed desorption of ammonia (NH_3-TPD), and low-temperature nitrogen adsorption-desorption. Among these catalysts Fe-ZSM-12 demonstrated the best activity: exhaustive oxidation of dibenzothiophene (DBT) in the presence of this catalyst was achieved in 2 h at 150°C. Influence of the reaction conditions (temperature, amount of catalyst, and time) on the conversion of the model substrate was studied. It was shown that in the presence of Fe-ZSM-12 catalyst activation of molecular oxygen proceeds via formation of superoxide radical. Fe-ZSM-12 exhibited an excellent stability and retained its activity after 10 cycles of oxidation. Under optimal reaction conditions sulfur content in straight-run gasoline fraction was reduced from 807 to 43 ppm, in diesel fraction – from 1898 to 150 ppm. Two-dimensional GC-MS analysis of diesel fraction before and after desulfurization indicates high selectivity of the process. Possibility of sulfur dioxide formation during the aerobic oxidative desulfurization process was studied for the first time. The use of zeolite-based catalysts containing transition metals for aerobic oxidation of sulfur-containing compounds is a promising approach for clean fuel production.

1. Introduction

Sulfur is one of the main petroleum heteroatoms. Sulfur compounds contained in motor fuels form toxic oxides during combustion, which have an extremely negative impact on the environment [1,2]. Therefore, in many countries strict requirements are introduced for the sulfur content in motor fuels, even at the ultra-low level (less than 10 ppm) in many cases [3,4]. At the same time, light oil reserves are steadily depleted worldwide, resulting in the need for intensified processing of heavy oil deposits with high sulfur content. In turn, this leads to an increase in the sulfur content in the produced oil fractions, which causes an overload of existing desulfurization processes: hydrodesulfurization (HDS) and hydrocracking. It should be noted that HDS process, which is widely used in oil refining, has low efficiency in removing aromatic sulfur compounds, especially dibenzothiophene and its substituted derivatives [5]. Meanwhile, condensed thiophene derivatives are widely represented in oil fractions, constituting the largest proportion of sulfur compounds in them. Therefore, along with the constant improvement of the traditional method of HDS the task of finding alternative ways to reduce the sulfur content in refined products is urgent [6].

The main hydrogen-free sulfur purification methods are adsorption [7], extraction [8,9], biodesulfurization [10], and oxidative desulfurization [11]. Among these methods, oxidative desulfurization technique is the main focus of the researchers' attention nowadays [12, 13]. This method allows to purify fuels under relatively mild conditions to ultra-low sulfur levels that meet the strict environmental standards. Over the past 20 years the number of publications on oxidative desulfurization has increased exponentially [14].

Oxidative desulfurization method is a two-stage process. The first stage is oxidation of sulfur compounds to the corresponding sulfoxides and sulfones. At the second stage, the oxidation products are selectively separated from the hydrocarbon medium via extraction or adsorption.

* Corresponding author at: Chemistry Department, Lomonosov Moscow State University, 119234 Moscow, Russia.
E-mail addresses: arvchem@yandex.ru (A.V. Akopyan), esevakatya@mail.ru (E.A. Eseva).

https://doi.org/10.1016/j.ceja.2022.100385

Available online 23 August 2022

Inorganic oxidants [15], organic peroxides [16–19], hydrogen peroxide [20,21], ozone [22,23], molecular oxygen [24–26], as well as air oxygen [27–29] are widely used as oxidants at the first stage. Using hydrogen peroxide as an oxidizing agent allows to carry out oxidative desulfurization under mild conditions (temperatures up to 80°C) which attracts a lot of attention to this technique. However, it still has a major drawback: as the sulfur content in the feed is growing yearly, the demand for hydrogen peroxide also increases accordingly. This limits the scaling-up of hydrogen peroxide-based desulfurization technology as the total cost of even such a relatively inexpensive oxidant becomes excessive at the industrial level.

In this regard, the use of atmospheric oxygen, the most accessible oxidizing agent among those studied, is the most interesting from the practical point of view. This prompted an increasing number of studies devoted to the development of catalytic systems for the oxidation of sulfur compounds with atmospheric oxygen (Table 1S, Supporting Information) [30].

Metal complexes, in particular iron [31,32] and cobalt [33] phthalocyanines, are used as catalysts for the oxidation of sulfur substrates and allow to achieve a high conversion of DBT (more than 90%). However, the use of such catalysts is limited due to their high cost. In this regard, transition metal oxides capable of catalyzing aerobic oxidation of organosulfur substrates are of great interest. The successful use of copper and zinc oxides modified with molybdenum oxide as catalysts for the oxidation of dibenzothiophene derivatives with yields of more than 80% was demonstrated earlier [34,35]. The key disadvantage of such systems is the high reaction temperature (more than 350°C). On the one hand, this drives up the cost of such purification due to high energy consumption, and on the other hand, reduces the selectivity of the process by increasing the rate of side reactions, for example, hydrocarbon components oxidation. The use of polyoxometalates as catalysts for aerobic oxidation can significantly reduce the reaction temperature (to less than 150°C) [36,37]. One of their disadvantages is the complicated synthesis procedure. Another significant drawback of these catalysts is their sensitivity to the hydrocarbon media, since they are highly active when using solvents containing a tertiary carbon atom (decalin, cumene, etc.) and practically inactive in normal alkanes (dodecane) [38]. Therefore, polyoxometalates exhibit low catalytic activity in aerobic oxidative desulfurization of real petroleum fractions containing a mixture of hydrocarbons.

In this regard, aerobic oxidation catalysts based on zeolite materials, many of which are produced on an industrial scale, are of considerable interest. In the work [39], copper and cobalt-containing catalysts based on Y-type zeolite were successfully used for the exhaustive oxidation of dibenzothiophene. Cobalt-containing catalyst based on ZSM-5 can be used for the oxidation of cyclohexanol with oxygen [40]. Fe-based catalysts are inexpensive, highly efficient, and nontoxic materials, which are widely used as catalysts for the aerobic oxidation of various organic substrates [41]. In particular, iron-based catalysts are actively utilized for the production and processing of biofuels [42], in the well-known Fischer-Tropsch process [43], and in the oxidation of benzyl hydrocarbons and alcohols [44, 45].

In this work, zeolite-based catalysts were successfully used for the exhaustive oxidation of sulfur-containing substrates with atmospheric oxygen in a model mixture containing dodecane as a solvent. The choice of the reaction medium is due to the lower tendency of normal alkanes to form oxygen-containing compounds. Thus, aerobic oxidation reactions proceed slowly in normal alkane medium. Therefore, catalysts that allow the aerobic oxidation of sulfur-containing substrates in normal alkanes should work even more efficiently in the aerobic oxidative desulfurization of real petroleum distillates, because the latter, in addition to normal alkanes, also contain various isomers, naphthenic and alkylaromatic hydrocarbons, which enhance aerobic oxidation reactions.

We synthesized a series of iron-containing catalysts based on ZSM-12 and ZSM-5 zeolites. A comparative analysis of the activity of synthesized catalysts in the process of aerobic oxidative desulfurization of a model fuel is presented. The possibility of using the synthesized catalysts for aerobic oxidative desulfurization of real oil fractions samples has been studied. The work demonstrates the influence of the reaction conditions (temperature, time, amount of catalyst, nature of the sulfur-containing compound) on the conversion of the substrate. The dependence of the process of oxidative desulfurization on the hydrocarbon composition of the diesel fraction was analyzed. In addition, the possibility of sulfur dioxide formation during the aerobic oxidative desulfurization process was studied for the first time.

2. Experimental

2.1. Catalyst preparation

Synthesis of zeolites Na-ZSM-5 and Na-ZSM-12 was carried out in accordance with the literature [46, 47]. The deposition of iron on zeolite samples was carried out by impregnation method on the sodium form of aluminosilicate with an aqueous solution of iron chloride (III). An aqueous solution of a transition metal (1.5 mmol of iron salt per 20 ml of distilled water with concentration of 0.08 M) was added to 1 g of zeolite and vigorously stirred for 3 h at room temperature and then for 3 h at 80°C. Next, the obtained iron-containing zeolite was separated by centrifugation, after that the impregnation procedure was repeated twice. The resulting catalysts were centrifuged, dried at room temperature overnight and then dried at 100°C and 110°C for 2 h at each temperature, followed by calcination at 550°C for 6 h. Samples were named Fe-ZSM-12 and Fe-ZSM-5.

2.2. Catalytic experiments

The feed model mixture was prepared by dissolving dibenzothiophene (DBT) in dodecane with total sulfur (S) content of 500 ppm. The catalyst was added to the flask in amount of 0.1–1 wt.%, and 30 ml of the model DBT feed mixture was continuously stirred for 2 h in an oil bath at 110–150°C and a stirring speed of 550 rpm. Air was bubbled through the reaction system using a glass porous tube at a rate of 6 l/h. Model feed mixture was analyzed by GC-FID with an absolute calibration method (Kristall 2000 M equipped with a capillary column (ZB-1 liquid phase, 30 $m \times 0.32$ mm).

Figs. 6–9 show the average values of the three converging results. The experimental error does not exceed 5%.

2.3. Catalytic desulfurization of real hydrocarbon feed

To 30 ml of petroleum oil (straight-run gasoline, diesel fraction) 1 wt.% catalyst was added, a tube was connected to bubbling an air flow at a rate of 6 l/h and the mixture was heated with stirring at the temperature of 150°C for 1–6 h. Upon completion of the reaction, the catalyst was separated from the hydrocarbon phase by centrifugation. The products of the oxidation reaction of the gasoline fraction were extracted using acetonitrile in a volume ratio of 1:1. Silica gel adsorption was used to extract the oxidation products of the diesel fraction.

Analysis of gasoline and diesel fractions was conducted by two-dimensional GC with time-of-flight mass spectrometry and flame ionization detection (GC × GC−TOFMS−FID) on a Leco Pegasus GC—HRT 4D. The instrument includes an Agilent 7890A gas chromatograph with an embedded second oven, a flow splitter, a flame ionization detector, a two-stage cryomodulator, and a Leco Pegasus 4D time-of-flight mass analyzer. Analysis results were processed using ChromaTOF software (Leco). Analysis conditions are given below:

- Injector: temperature, 300°C; sample volume, 0.2 μL; carrier gas, helium; flow rate through the column, 1 mL/min; split ratio, 500; injector (septum) purge flow rate, 3 mL/min; and operating mode, pressure adjusted to maintain a constant flow rate.

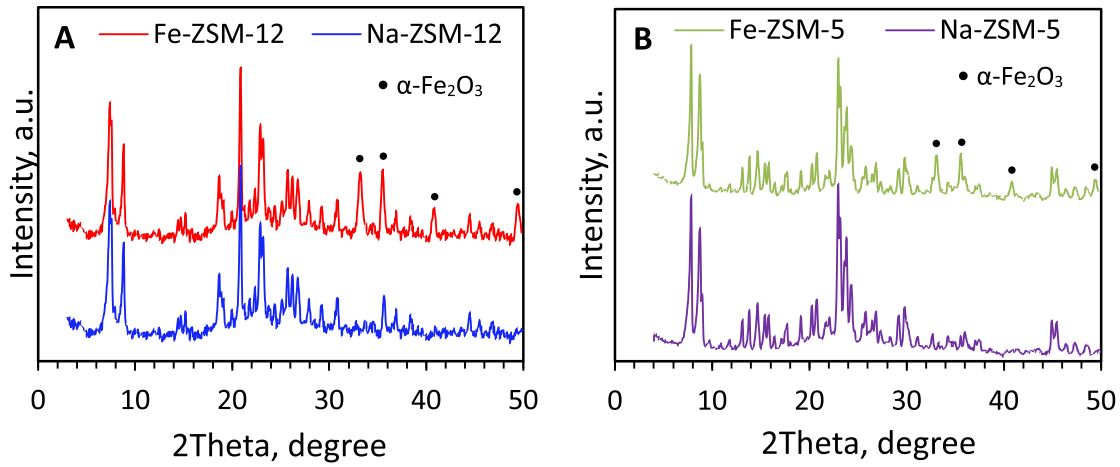

Fig. 1. X-ray diffraction patterns of zeolites Na-ZSM-12 (A), Na-ZSM-5 (B) and respective iron-containing catalysts.

Table 1
Elemental analysis and texture properties of the obtained catalysts.

Sample	Amount found,% mass.					Si/Al	Crystallinity[1],%	Fe_2O_3 size[2], Å	S_{BET}[3], m^2/g	V_{MICRO}, cm^3/g
	Si	*Al*	*Fe*	*Na*	*Cl*					
Na-ZSM-5	45.05	1.35		0.13		64	90	–	457	0.116
Fe-ZSM-5	45.6	1.34	3.1	–	0.03	57	88	290	321	0.076
Na-ZSM-12	45.74	0.88	–	0.24	–	100	70	–	271	0.103
Fe-ZSM-12	43.80	0.85	3.0	–	0.02	99	65	210	240	0.084

[1] The degree of crystallinity was calculated from the ratio between the areas (integral intensities) of peaks associated with the crystalline and amorphous phases.
[2] Calculated by Scherrer's equation.
[3] Brunauer-Emmett-Teller method (BET).

- Chromatographic separation: column 1, polar; phase, Rxi-17Sil (30 *m* × 0.25 mm × 0.25 μm); column 2, nonpolar; and phase, Rxi-5Sil (1.7 *m* × 0.10 mm × 0.10 μm). Temperature regime of the first oven: initial temperature, 40 °C (2 min); heating to 320°C at a rate of 3°C/min; and holding for 5 min. The second oven temperature and the modulator are maintained at levels of 6 and 21°C higher than the temperature of the first oven, respectively. Modulation time on the modulator is 6 s.
- Flame ionization detector: temperature, 340°C; H_2 flow rate, 40 mL/min; air flow rate, 450 mL/min; and blowing in flow rate, 30 mL/min. The line to the detector is 1.4 m × 0.25 mm; the first oven sets the temperature.
- Mass detector: ion source temperature, 280°C; frequency, 100 Hz; detected mass range, 35−520; recording rate, 100 spectra per second; and electron energy, 70 eV. The line to the detector is 3.0 m × 0.18 mm and temperature, 280°C.

3. Results and discussions

3.1. Catalysts characterization

Crystal structure of the initial zeolites and synthesized catalysts was studied by X-ray diffraction analysis. Comparison of the catalysts' XRD spectra with those of initial zeolite samples indicates that the crystallinity and the structure of the zeolite matrix are retained after the deposition of metals on its surface (Fig. 1). The peaks of the initial Na-ZSM-12 correspond to the material with a monoclinic system, space group *C/2c*. The phase of Na-ZSM-12 zeolite was identified by the main characteristic peaks at 2θ = 7.5°, 8.9°, 20.9°, 25.9°, and 35.8°, attributed to the crystal faces (200), (−202), (310), (−513), and (−518), accordingly [46, 48]. The structure of Na-ZSM-5 is orthorhombic (space group *Pnma*). Characteristic reflections of ZSM-5 at 2θ = 7.9°, 8.7°, 22.9°, 23.8° and 24.2° correspond to the (101), (020), (501), (151) and

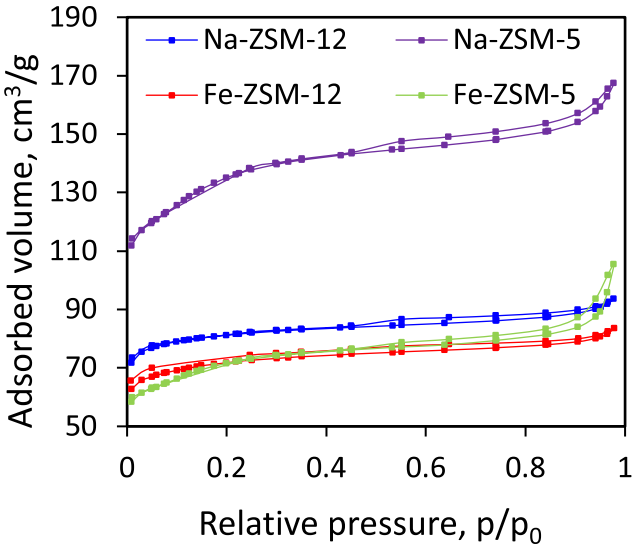

Fig. 2. Low-temperature N_2 adsorption-desorption isotherms of zeolite-based catalysts.

(303) crystal faces, respectively [49]. In addition, the appearance of reflections at 2θ = 33.08°, 35.56°, 40.76°, 49.4° in the X-ray diffraction spectrum of iron-containing samples is related to the structure of α-Fe_2O_3 [50]. A slight decrease in the intensity of the peaks of Fe-ZSM-5 and Fe-ZSM-12 catalysts can be associated with the redistribution of ions after the metabolic processes.

In addition, the evaluation of Fe_2O_3 particle size using the Scherrer equation (Table 1) was provided. According to XRD data, average Fe_2O_3 particle sizes in Fe-ZSM-5 and Fe-ZSM-12 are 290 and 210 Å, respectively.

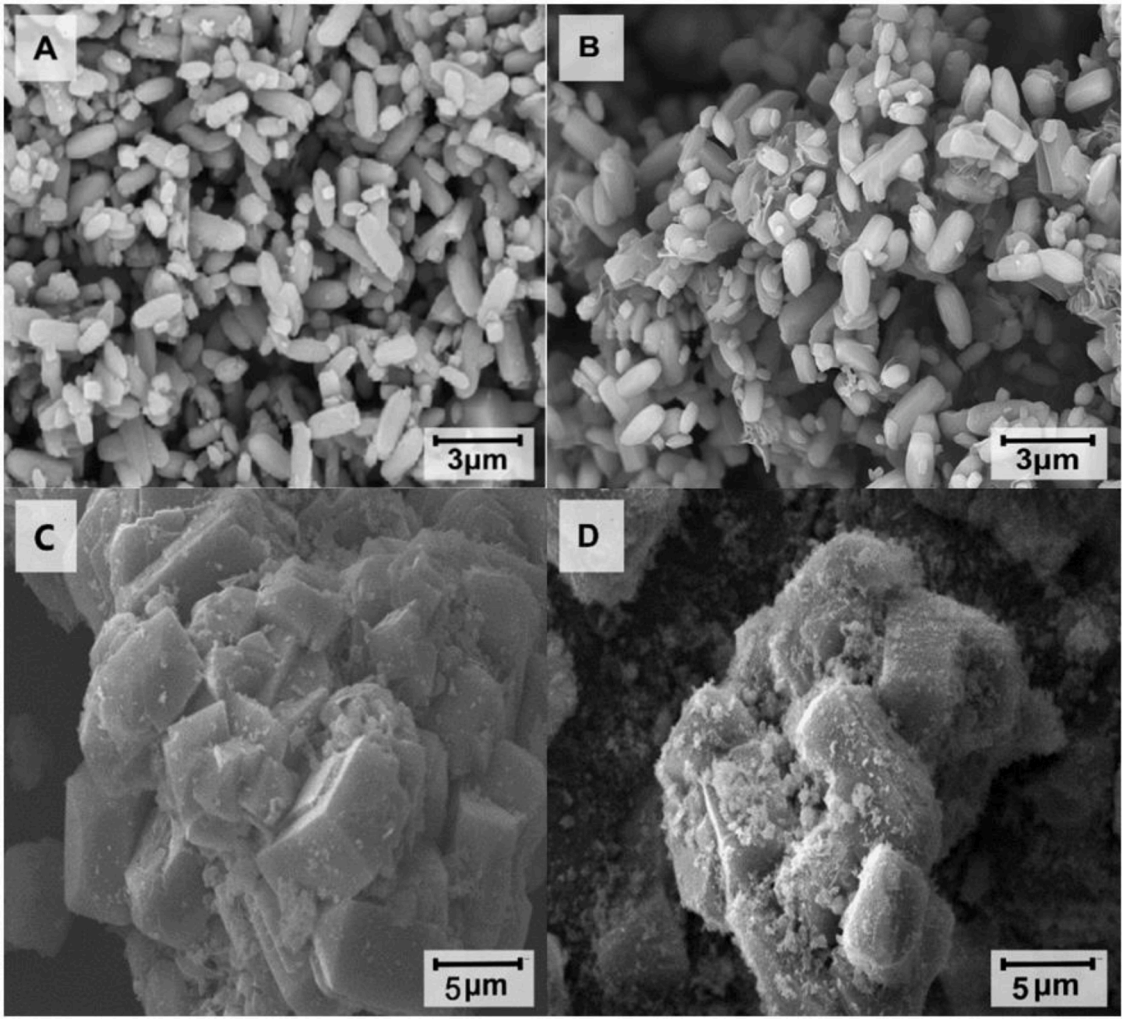

Fig. 3. Micrographs of scanning electron spectroscopy of the Na-ZSM-12 (A), Fe-ZSM-12 (B), Na-ZSM-5 (C) and Fe-ZSM-5 (D).

Structural and textural characteristics of the initial zeolites and synthesized catalysts were studied by the low-temperature nitrogen adsorption-desorption method. As shown in Fig. 2, all samples have a type I isotherm curve without a hysteresis loop, which is characteristic of microporous solids. In the region of low relative pressures (p/p_0 = 0.01–0.25) abrupt adsorption of nitrogen is observed, which confirms the presence of micropores in the structure of the original zeolites [51].

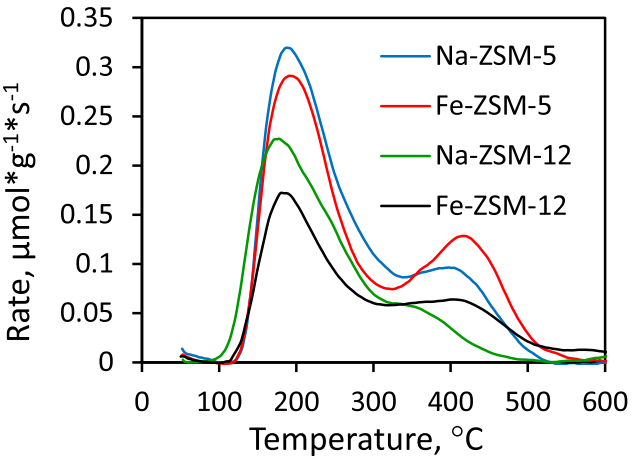

Fig. 4. Acidity of zeolite materials and iron-containing catalysts.

Zeolite Na-ZSM-5 has a higher nitrogen uptake in the low-pressure region compared to Na-ZSM-12 zeolite, indicating higher values of its specific surface area (Table 1). Deposition of metal on the zeolite surface leads to a decrease in the amount of adsorbed nitrogen associated with the blocking of pores and channels in the zeolite structure, which is in good agreement with the XRD data. Nevertheless, the iron-containing samples still have high surface areas and pore volume, and the corresponding isotherms are typical for microporous solids.

Metal content in the obtained catalysts was estimated by the elemental analysis (Table 1). The results show that the content of iron after the deposition is 3 wt.%. According to the results, the sodium content in the structure of the obtained catalysts decreases, which confirms the exchange reactions between cations in an aqueous solution. It should also be noted, that iron particles are deposited on the surface of the support in the form of physically adsorbed particles. Thus, the presented procedure for the synthesis of catalysts makes it possible to carry out both cation exchange and the deposition of iron particles on the support surface.

It should be noted, that according to the elemental analysis data, obtained Si/Al ratio in the synthesized catalysts is lower than the calculated one. This may occur due to incomplete transition of silicon dioxide from the colloidal form to the crystalline phase during the crystallization process. This effect was also observed in a number of other works [52, 53]. Small deviations from the original zeolite samples can be associated with measurement error, which is 5% for elemental analysis. The degree of crystallinity calculated by the X-ray diffraction

Table 2
The NH_3 adsorption capacity of obtained zeolite-based catalysts and original zeolites.

Sample	Peak position (°C)		NH_3 desorbed (μmol/g)		
	Weak acid	*Strong acid*	*Weak acid*	*Strong acid*	*Total acid*
Na-ZSM-5	188	398	279	91	370
Fe-ZSM-5	190	415	235	129	364
Na-ZSM-12	182	354	204	85	289
Fe-ZSM-12	184	403	140	92	232

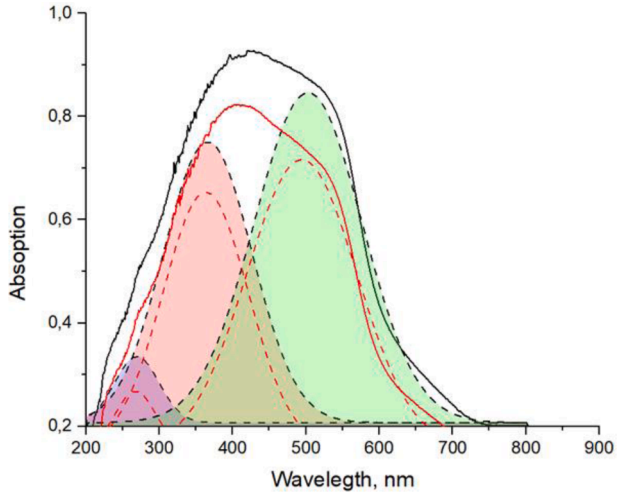

Fig. 5. UV–Vis spectra of Fe-ZSM-12 (black) and Fe-ZSM-5 (red line).

method for the initial ZSM-5 zeolite is 90%, and for its iron-containing derivative it does not exceed 88%. In the case of ZSM-12, the crystallinity in the initial sample is 70%, while after deposition of transition metals it ranges from 65 to 68%. The drop in crystallinity in the resulting catalysts may be associated both with the formation of an amorphous phase during synthesis and with a measurement error.

Fig. 3 demonstrates micrographs of the obtained zeolites and iron-containing catalysts based on them. The initial Na-ZSM-5 zeolite sample exhibits typical hexagonal crystal morphology and has a smooth angular surface [54]. Na-ZSM-12 is characterized both by small particles similar in shape to rice grains and large elongated cubic crystals [55]. Crystallites have a wide distribution of sizes and shapes. The structure of zeolite materials remains unchanged after the iron deposition stage, which is in good agreement with the results of X-ray phase analysis.

Total acidity of initial zeolites and iron-containing catalysts based on them was studied by NH_3-TPD (Fig. 4). Table 2 shows the concentrations of weak (100–300°C) and strong (300–500°C) acid sites as well as their total content. Different acidity is observed for Na-ZSM-5 and Na-ZSM-12 which is associated with different synthesis parameters, structure of the zeolite material, and the Si/Al ratio. It was found that after the deposition of iron the concentration of weak acid sites decreases, while the concentration of strong sites slightly increases. In addition, the encapsulation of iron particles leads to a slight change in the total acidity. The change in the content of acid sites is associated with the appearance of additional acid sites due to the formation of an iron oxide phase [56].

Fig. 5 shows the diffuse reflectance spectra of both iron-containing zeolite-based catalysts, which were used to evaluate the nature of iron particles. The band at about 250 nm corresponds to isolated octahedral or pseudo tetrahedral coordinated Fe^{3+} ions. The band in the wavelength range of 300 nm $< \lambda <$ 400 nm indicates the presence of small $Fe_x^{3+}O_y$ clusters in the sample, while the band in the region after 400 nm is characteristic of larger Fe_2O_3 particles [56]. As can be seen, the spectra of both iron-containing zeolite-based catalysts are identical, which means that the nature of iron centers does not depend on the zeolite type.

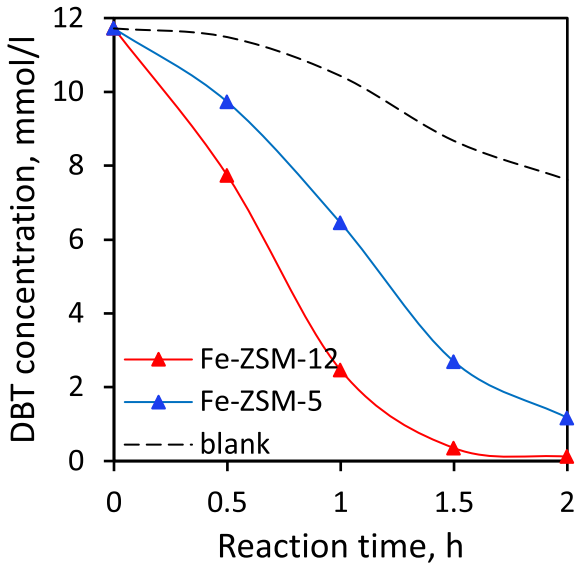

Fig. 6. Comparison of the catalytic activity of synthesized iron-containing catalysts based on zeolites. Reaction conditions: 500 ppm S in model feed, 150°C, 1% mass. Catalyst, 6 l/h, 550 rpm.

3.2. Catalytic experiments

Catalytic activity was studied on a model mixture of DBT in dodecane with an initial sulfur content of 500 ppm. According to the results (Fig. 6), the catalyst Fe-ZSM-12 is more catalytically active in the aerobic oxidation, as it allows to achieve complete removal of DBT in 2 h. In the presence of Fe-ZSM-5 the rate of substrate oxidation is also high, but somewhat less than in the case of Fe-ZSM-12. It can also be seen that the concentration of DBT decreases by 35% in 2 h in the reaction without a catalyst resulted from the oxidation by alkyl peroxides generated in the reaction of the solvent with air oxygen. Taking into account that the dimensions of the pores and channels of the support are much smaller than those of the substrates (ZSM-5: 5.3 × 5.6 Å, ZSM-12: 5.7 × 6.1 Å, DBT: 6.1 × 9.8 Å), it can be assumed that the catalytic reaction predominantly proceeds on the outer surface of the zeolite. This includes adsorption of substrate molecules on the catalyst surface, their interaction with active sites, and further desorption. The addition of iron particles to the system accelerates the oxidative reaction, which is associated with the ability of the transition metal to activate molecular oxygen by the formation of free radicals.

The difference in the activity between Fe-ZSM-5 and Fe-ZSM-12 can be explained by the different acidity of the supports. The catalyst based on ZSM-5 with a higher acidity exhibits lower catalytic activity. These results are in good agreement with the known literature data, according to which an increase in the basic properties of the catalyst improves the course of aerobic oxidation reactions. Considering that the reaction proceeds on the outer surface of the catalyst particles, the difference in the activity of the two catalysts can also be due, among other things, to the different morphology of the zeolite crystals [57, 58].

The catalyst based on ZSM-12 zeolite was also synthesized by only one impregnation cycle, in that case the content of supported iron was lower – 1.5 wt.%, according to the results of elemental analysis. The content of metal directly affects the catalytic activity of the obtained catalyst, as the DBT conversion did not exceed 60% in 2 h under identical oxidation conditions. The Fe-ZSM-12 catalyst was chosen for further experiments due to its higher activity and availability of iron.

Fig. 7(A) shows the temperature dependence of the dibenzothiophene conversion. The reaction temperature has a significant effect on the rate of substrate oxidation. Thus, a decrease in temperature from

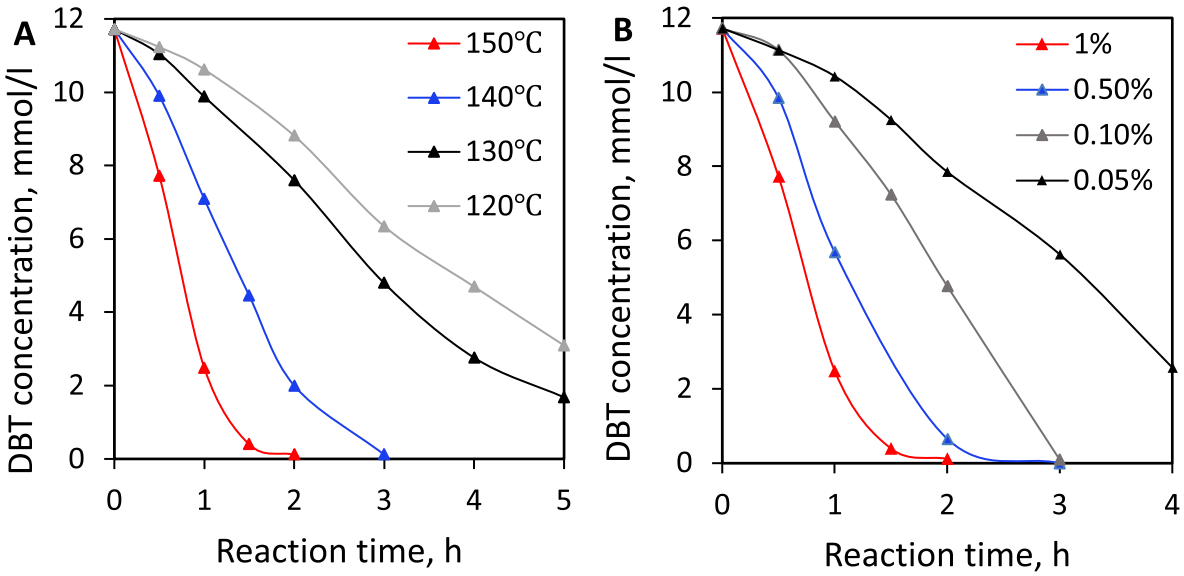

Fig. 7. (A) Effect of temperature. Reaction conditions: 1 wt.% catalyst, 6 l/h, 550 rpm. (B) Effect of catalyst amount on DBT conversion. Reaction conditions: 150°C, 6 l/h, 550 rpm.

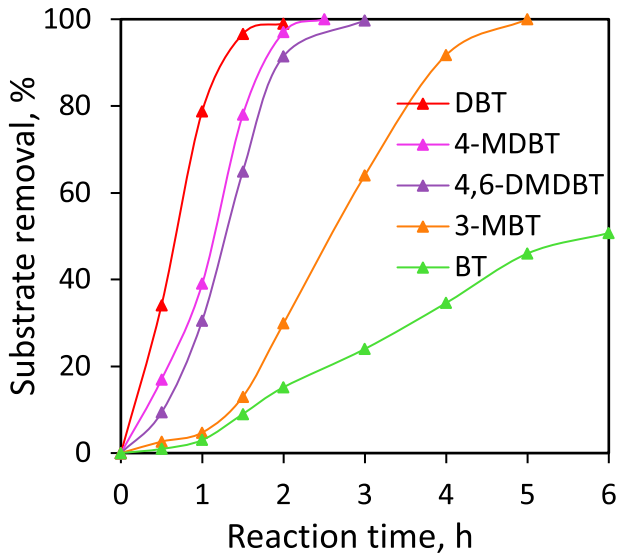

Fig. 8. Oxidation of various sulfur-containing substrates. Reaction conditions: 150°C, 1 wt.% catalyst, 6 l/h, 550 rpm.

150°C to 120°C in increments of 10° leads to a slow drop in the DBT conversion rate. The lower the temperature, the smoother the dependence curve. The temperature of the oxidation process affects the generation rate of oxygen-containing particles under the influence of atmospheric oxygen. Fe-ZSM-12, in its turn, participates in the decomposition of the generated particles to a superoxide radical and directs them to the oxidation of sulfur-containing molecules. With a drop in the reaction temperature, the rate of particle generation decreases sharply; therefore, a much smaller number of radicals directed to the interaction with the substrate is formed. Further experiments were carried out at a temperature of 150°C characterized by the highest DBT oxidation reaction rate, since this value can also be easily achieved in oil refining. Fig. 7(B) exhibits the results of DBT oxidation at various catalyst loadings. The decrease in the amount of catalyst leads to the decrease in the rate of DBT oxidation. Nevertheless, even with a reduced loading (0.5 and 0.1%) it is possible to achieve an exhaustive oxidation of DBT in 3 h.

To scale up the aerobic oxidation process to a real hydrocarbon feedstock, it is necessary to study the reactivity of various classes of sulfur-containing compounds. The activity of organosulfur substrates decreases in the order of DBT > 4-MDBT (4-methyldibenzothiophene) > 4,6-DMDBT (4,6-dimethyldibenzothiophene) > 3-MBT (3-methylbenzothiophene) > BT (benzothiophene) (Fig. 8). According to the results obtained, the reactivity of sulfur-containing compounds depends on the two main factors: the electron density on the sulfur atom and steric hindrances, which is in a good agreement with the published data [59].

In order to understand how the synthesized catalyst activates molecular oxygen, oxidation was carried out with the addition of quenchers for radicals that can be formed under the reaction conditions. According to the literature [60], benzoquinone, potassium iodide and sodium azide are quenchers for superoxide radical, OH• radical and singlet oxygen, respectively. It should be noted that the addition of each of these quenchers leads to a decrease in DBT conversion (Fig. 9(A)). Nevertheless, the maximum decrease in DBT conversion is achieved in the presence of benzoquinone, which indicates the predominant role of the superoxide radical in the aerobic oxidation of organosulfur substrates in the presence of Fe-ZSM-12.

The results on the use of the catalyst in the recycle mode are demonstrated in Fig. 9(B). Fe-ZSM-12 retained high activity during 10 oxidation cycles: DBT conversion decreases by only 2%, which is within the statistical experimental error of 5%.

After 10 oxidation cycles Fe-ZSM-12 was separated from the reaction mixture, washed with ethyl alcohol from the remains of the model mixture, dried at 100°C, and then analyzed by XRF and XRD methods. According to the XRF results, the iron content in the spent catalyst is 3 ± 0.01%, which indicates that there was no leaching of the active phase under the oxidation conditions. At the same time, a comparison of the XRD spectra of the fresh and the used catalysts (Fig. 10) suggests that the zeolite structure does not undergo destruction or any other changes during the reaction course. Thus, the synthesized catalyst not only has an excellent catalytic activity, but also shows high stability under the conditions of aerobic oxidation of organosulfur substrates.

Two-dimensional GC–MS analysis of the model mixture before and after aerobic oxidation indicates that the only oxidation product of dibenzothiophene is the corresponding sulfone (Fig. 1S, Supporting Information). It should be noted, that dodecane oxidation products, particularly corresponding alcohols and ketones, are detected in the mixture after the oxidation reaction. It is important that the occurrence

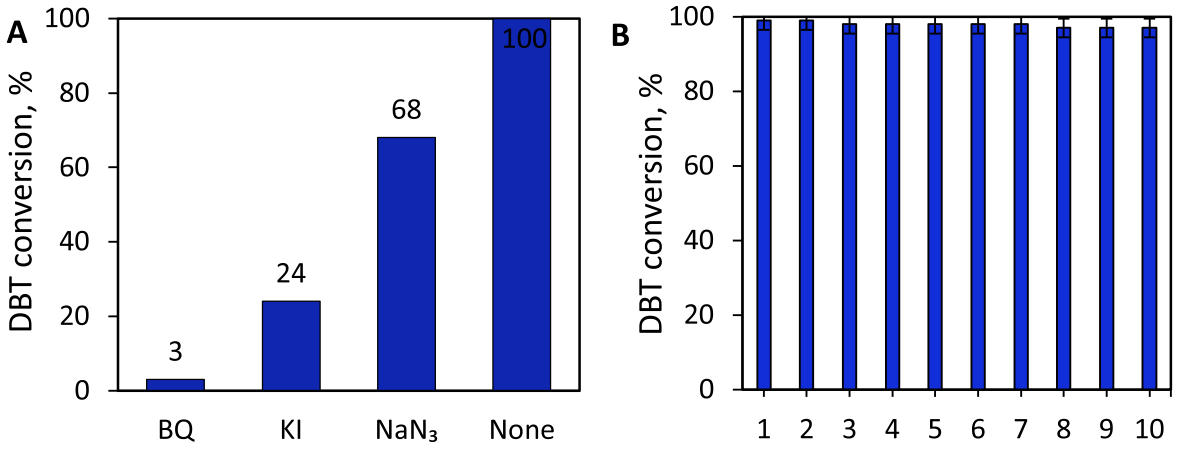

Fig. 9. (A) The effect of radical quenchers on DBT conversion. Reaction conditions: 150°C, 3 h, 0.5% mass. catalyst, 6 l/h, 550 rpm. (B) Effect of catalyst recycling on the DBT conversion. Reaction conditions: 150°C, 0.5% mass. catalyst, 3 h, 6 l/h, 550 rpm.

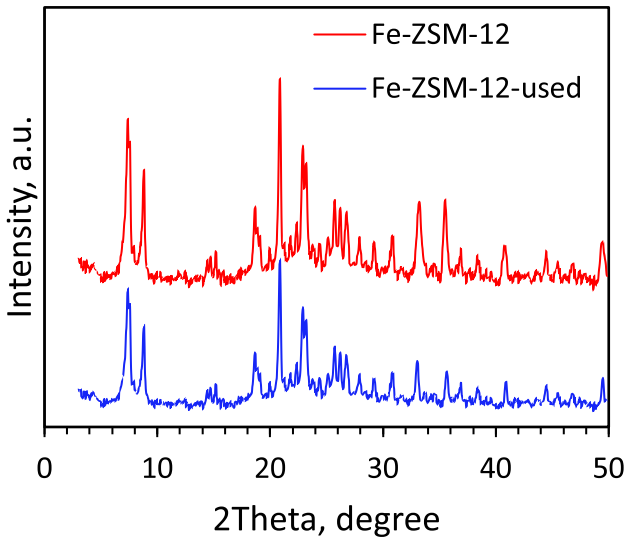

Fig. 10. X-ray diffraction patterns of freshly prepared and regenerated zeolite samples Fe-ZSM-12.

Table 3
Determination SO_2 by ISO 7934.

Time, h	*SO_2 concentration, ppm*	
	150°C	*200°C*
1	0	0
3	0	0
6	0	0

of side reactions is insignificant and carboxylic acids are not formed as a result, which suggests that oxidation of dodecane to carbon dioxide also does not take place.

The fact that the further oxidation of the corresponding dibenzothiophene sulfone to sulfur dioxide does not occur was confirmed by analyzing the exhaust air for SO_2 using the ISO 7934 method (Fig. 2S, Supporting Information).

The experiments were carried out both at a reaction temperature of 150°C and at an elevated temperature of 200°C. A further increase in temperature in the open system was impossible, because of the boiling point of dodecane (216°C). Obtained data indicates that no detectable amounts of sulfur dioxide were found (Table 3). This fact is in accordance with the literature [61], which denotes the beginning of decomposition of dibenzothiophene sulfone at temperatures above 300°C.

Oxidative desulfurization of the real samples of straight-run gasoline and diesel fractions was carried out in the presence of the synthesized Fe-ZSM-12 catalyst (Fig. 11). In the gasoline sample the total sulfur content was reduced from 807 ppm to 43 ppm, while in the straight-run diesel sample it was reduced from 1898 ppm to 150 ppm. Obtained results demonstrate that the synthesized catalyst allows to carry out aerobic oxidative desulfurization not only in model mixtures, but also in real oil fractions.

The effect of oxidative desulfurization on the hydrocarbon composition was evaluated for the diesel fraction, since the naphthalene derivatives and polyaromatic compounds contained in this fraction are most sensitive to oxidation by atmospheric oxygen. The results of two-dimensional gas chromatography-mass spectrometric analysis of the diesel fraction before and after the process of aerobic oxidative desulfurization indicate that there were no significant changes in the hydrocarbon composition (Fig. 12).

After desulfurization, the content of polyaromatic compounds was reduced by 2%, while the content of other classes of hydrocarbon components (alkanes, cycloalkanes, monoaromatic compounds) remained unchanged (Table 4). This confirms high selectivity of the developed catalyst towards sulfur-containing compounds.

4. Conclusions

Iron-containing catalysts based on zeolites ZSM-5 and ZSM-12 were synthesized and applied for the first time for highly efficient aerobic oxidation of model mixtures and real fuels. The catalysts' structure and composition were investigated by XRD, XRF, SEM, UV–Vis, and low-temperature N_2 adsorption-desorption techniques. Comparison of the XRD spectra indicates that the crystallinity and structure of the zeolite matrix are maintained after the deposition of metals on its surface. According to the elemental analysis by XRF, the content of the main elements (Si, Al) included in the framework of zeolite structure remains constant, which confirms the retention of the structure after the deposition of the metals.

The influence of the zeolite type, reaction temperature, catalyst loading, as well as the nature of sulfur-containing substrate on the reaction rate was investigated in detail. Complete oxidation of DBT was achieved in the presence of Fe-ZSM-12 catalyst under the following conditions: 2 h, 150°C, 1 wt.% catalyst loading, air flow rate 6 l/h. Addition of radical quenchers to the reaction system allows to conclude that the activation of molecular oxygen proceeds mainly via the formation of superoxide radical.

Fe-ZSM-12 catalyst showed an excellent stability and retained its

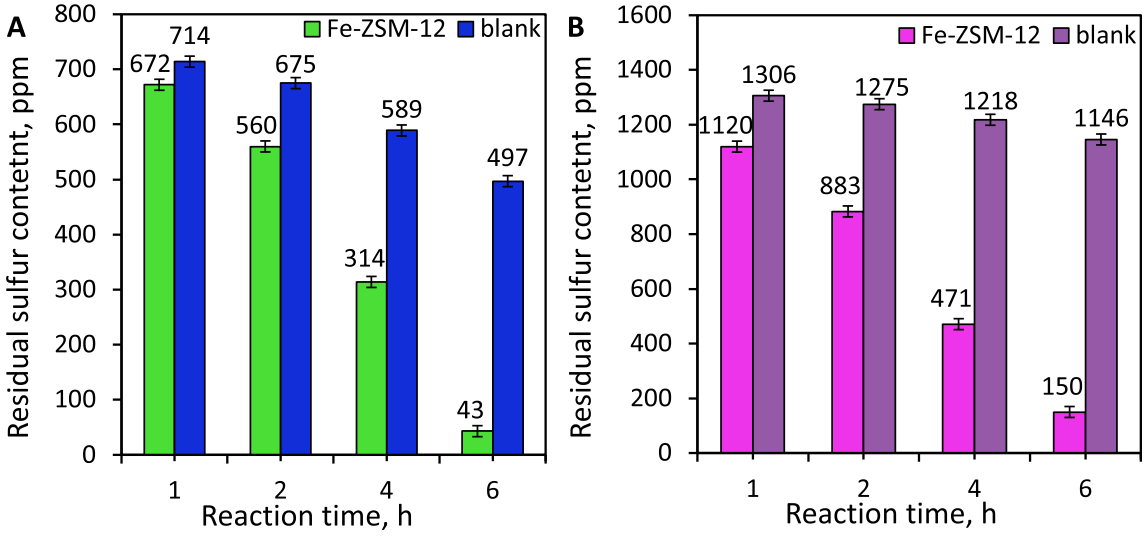

Fig. 11. Oxidation of real hydrocarbon feed (A) naphtha and (B) diesel. Reaction conditions: 150°C, 1% mass. catalyst, 6 l/h, 550 rpm. Residual sulfur content after blank naphtha extraction with acetonitrile: 758 ppm. Residual sulfur content after blank diesel adsorption on silica: 1315 ppm.

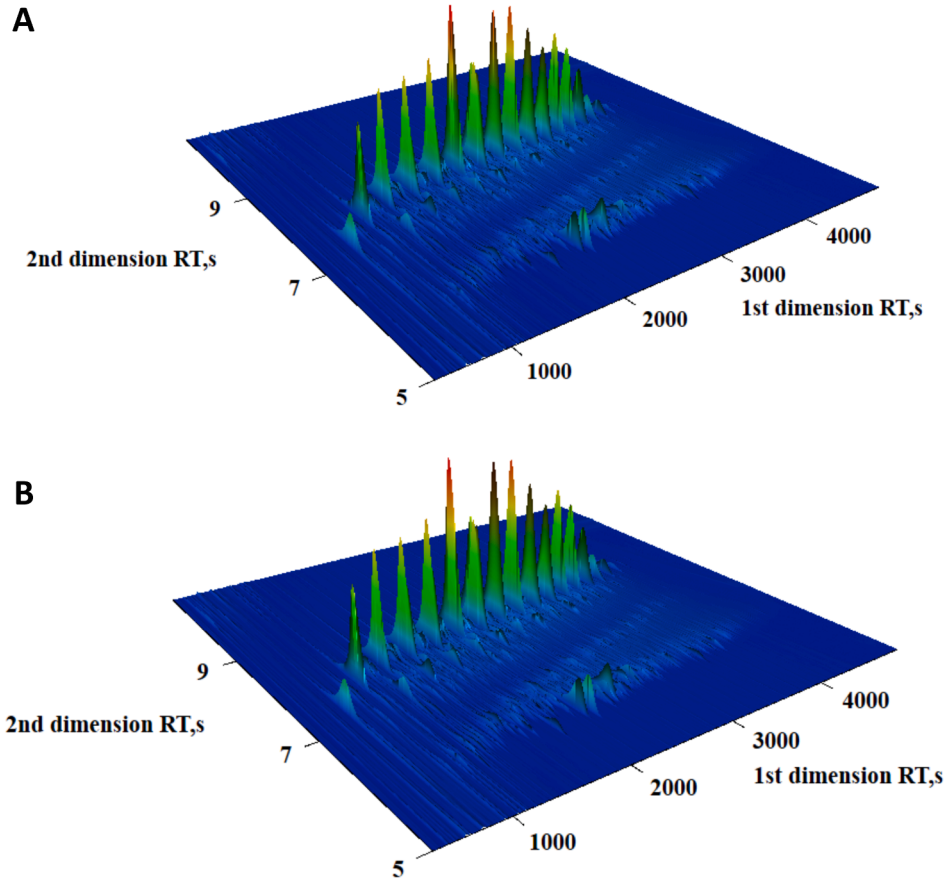

Fig. 12. 3D-chromatograms of raw diesel (A) and products after desulfurization (B).

activity after 10 cycles of oxidation without any changes in structure or leaching of the active sites. It was shown for the first time that the formation of sulfur dioxide does not occur under the conditions of aerobic oxidation reaction.

The possibility of the Fe-ZSM-12 use for oxidative desulfurization of real oil fractions samples was demonstrated. Under optimal conditions, the sulfur content in straight-run gasoline fraction was reduced from 807 to 43 ppm, in diesel fraction – from 1898 to 150 ppm. Two-dimensional GC–MS analysis of the diesel fraction before and after desulfurization shows that the hydrocarbon composition of the diesel fraction hardly changes in the process of aerobic oxidative desulfurization, which indicates a high selectivity of the process. The use of zeolite-based catalysts containing transition metals for aerobic oxidation of sulfur-containing compounds is a promising approach for clean fuel

Table 4
The content of the main classes of compounds in diesel fraction.

Class of compounds	*Content in raw diesel, wt%*	*Content in treated diesel, wt%*
Alkanes	47	49
Cycloalkanes	27	27
Monoaromatics	16	16
Polyaromatics	10	8

production. The results obtained in this work can be used in the development of a wide range of highly efficient and selective zeolite-based transition metal catalysts for the aerobic oxidative desulfurization of various oil fractions and other processes associated with it.

Supporting information

Comparison of various catalysts in the aerobic desulfurization reaction (Table 1S); Chromatogram of mass-spectrometry analysis (Fig. 1S); Laboratory setup for the determination of sulfur dioxide (Fig. 2S).

Author contributions

The manuscript was written through the contributions of all authors. All authors have given approval to the final version of the manuscript.

Funding sources

This research did not receive any specific grant from funding agencies in the public, commercial, or not-for-profit sectors.

Declaration of Competing Interest

The authors declare that they have no known competing financial interests or personal relationships that could have appeared to influence the work reported in this paper.

Supplementary materials

Supplementary material associated with this article can be found, in the online version, at doi:10.1016/j.ceja.2022.100385.

References

[1] H. Yang, B. Jiang, Y. Sun, L. Zhang, Z. Sun, J. Wang, X. Tantai, Polymeric cation and isopolyanion ionic self-assembly: novel thin-layer mesoporous catalyst for oxidative desulfurization, Chem. Eng. J. 317 (2017) 32–41, https://doi.org/10.1016/j.cej.2017.01.135.
[2] R. Zhao, J. Wang, D. Zhang, Y. Sun, B. Han, N. Tang, J. Zhao, K. Li, Deep catalytic oxidative desulfurization of model fuel based on modified iron porphyrins in ionic liquids: anionic ligand effect, ACS Sustain. Chem. Eng. 5 (2017) 2050–2055, https://doi.org/10.1021/acssuschemeng.6b02916.
[3] D. Julião, A. Gomes, L. Cunha-Silva, R. Valença, J.C. Ribeiro, M. Pillinger, B. Castro, I.S. Gonçalves, S.S. Balula, A sustainable peroxophosphomolybdate/H_2O_2 system for the oxidative removal of organosulfur compounds from simulated and real high-sulfur diesels, Appl. Catal., A 589 (2020), 117154, https://doi.org/10.1016/j.apcata.2019.117154.
[4] M. Breysse, D. Mariadassou, S. Pessayre, C. Geantet, M. Vrinat, G. Perot, M. Lemaire, Deep desulfurization: reactions, catalysts and technological challenges, Catal. Today 84 (2003) 129–138, https://doi.org/10.1016/S0920-5861(03)00266-9.
[5] Z. Yu, X. Lü, S. Xun, M. He, L. Zhu, H. Chen, M. Yuan, L. Fan, W. Zhu, High-index planes T-Nb_2O_5 using self-assembly strategy for aerobic oxidative desulfurization in fuels, Fuel 307 (2022), 121877, https://doi.org/10.1016/j.fuel.2021.121877.
[6] Y.S. Tian, J. Long, J.W. Cui, W. Jin, D.L. Zeng, Ultra-deep oxidative desulfurization of fuel with H_2O_2 catalyzed by phosphomolybdic acid supported on silica, Chinese J. Catal. 37 (2016) 2098–2105, https://doi.org/10.1016/S1872-2067(16)62558-5.
[7] F. Tian, Q. Shen, Z. Fu, Y. Wu, C. Jia, Enhanced adsorption desulfurization performance over hierarchically structured zeolite Y, Fuel Process. Technol. 128 (2014) 176–182, https://doi.org/10.1016/j.fuproc.2014.07.018.
[8] B. Rodríguez-Cabo, H. Rodríguez, E. Rodil, A. Arce, A. Soto, Extractive and oxidative-extractive desulfurization of fuels with ionic liquids, Fuel 117 (2014) 882–889, https://doi.org/10.1016/j.fuel.2013.10.012.
[9] D. Chandran, M. Khalida, R. Walvekar, N.M. Mubarak, S. Dharaskar, W.Y. Wong, T. C.S.M. Gupta, Deep eutectic solvents for extraction-desulphurization: a review, J. Mol. Liq. 275 (2019) 312–322, https://doi.org/10.1016/j.molliq.2018.11.051.
[10] M.A. Dinamarca, A. Rojas, P. Baeza, G. Espinoza, C. Ibacache-Quiroga, J. Ojeda, Optimizing the biodesulfurization of gas oil by adding surfactants to immobilized cell systems, Fuel 116 (2014) 237–241, https://doi.org/10.1016/j.fuel.2013.07.108.
[11] J. Xiao, L. Wu, Y. Wu, B. Liu, L. Dai, Z. Li, Q. Xia, H. Xi, Effect of gasoline composition on oxidative desulfurization using a phosphotungstic acid/activated carbon catalyst with hydrogen peroxide, Appl. Energ. 113 (2014) 78–85, https://doi.org/10.1016/j.apenergy.2013.06.047.
[12] A. Li, H. Song, H. Meng, Y. Lu, C. Li, Peroxovanadic based core-shell bifunctional poly(ionic liquid)s catalyst CuO/SiO_2@V-PIL: its in-situ free radical initiation mechanism for air oxidative desulfurization, Fuel 310 (2022), 122430, https://doi.org/10.1016/j.fuel.2021.122430.
[13] Q. Zhang, J. He, X. Fu, S. Xie, R. Fan, H. Lai, W. Cheng, P. Ji, J. Sheng, Q. Liao, W. Zhu, H. Li, Fluorine-free strategy for hydroxylated Ti_3C_2/Ti_3AlC_2 catalysts with enhanced aerobic oxidative desulfurization and mechanism, Chem. Eng. J. 430 (2022), 132950, https://doi.org/10.1016/j.cej.2021.132950.
[14] S. Houda, C. Lancelot, P. Blanchard, L. Poinel, C. Lamonier, Oxidative desulfurization of heavy oils with high sulfur content: a review, Catalysts 8 (2018) 344–370, https://doi.org/10.3390/catal8090344.
[15] S. Hongyan, G. Jiajun, C. Xingyu, H. Jing, Catalytic oxidation-extractive desulfurization for model oil using inorganic oxysalts as oxidant and Lewis acid-organic acid mixture as catalyst and extractant, Appl. Catal., A 456 (2013) 67–74, https://doi.org/10.1016/j.apcata.2013.02.017.
[16] X. Zhou, C. Zhao, J. Yang, S. Zhang, Catalytic oxidation of dibenzthiophene using cyclohexanone peroxide, Energy Fuels 21 (2007) 7–10, https://doi.org/10.1021/ef060441p.
[17] W.N.W. Abdullah, R. Ali, W.A.W.A. Bakar, In depth investigation of Fe/MoO_3–PO_4/Al_2O_3 catalyst in oxidative desulfurization of Malaysian diesel with TBHP-DMF system, J. Taiwan Inst. Chem. Eng. 58 (2016) 344–350, https://doi.org/10.1016/j.jtice.2015.06.001.
[18] J. Zou, Y. Lin, S.H. Wu, Y.Y. Zhong, C.P. Yang, Molybdenum dioxide nanoparticles anchored on nitrogen-doped carbon nanotubes as oxidative desulfurization catalysts: role of electron transfer in activity and reusability, Adv. Funct. Mater. 31 (2021), 2100442, https://doi.org/10.1002/adfm.202100442.
[19] J. Zou, Y. Lin, S. Wu, M. Wu, C. Yang, Construction of bifunctional 3-D ordered mesoporous catalyst for oxidative desulfurization, Sep. Purif. Technol. 264 (2021), 118434, https://doi.org/10.1016/j.seppur.2021.118434.
[20] J.L. García-Gutiérrez, G.C. Laredo, P. García-Gutiérrez, F. Jiménez-Cruz, Oxidative desulfurization of diesel using promising heterogeneous tungsten catalysts and hydrogen peroxide, Fuel 138 (2014) 118–125, https://doi.org/10.1016/j.fuel.2014.07.049.
[21] P. Polikarpova, A. Akopyan, A. Shigapova, A. Glotov, A. Anisimov, E. Karakhanov, Oxidative desulfurization of fuels using heterogeneous catalysts based on MCM-41, Energy Fuels 32 (2018) 10898–10903, https://doi.org/10.1021/acs.energyfuels.8b02583.
[22] W. Jianlong, Z. Dishun, K. Li, Oxidative desulfurization of dibenzothiophene using ozone and hydrogen peroxide in ionic liquid, Energy Fuels 24 (2010) 527–529, https://doi.org/10.1021/ef901324p.
[23] C. Ma, D. Bin, P. Liu, Deep oxidative desulfurization of model fuel using ozone generated by dielectric barrier discharge plasma combined with ionic liquid extraction, J. Ind. Eng. Chem. 34 (2013) 1014–1019, https://doi.org/10.1016/j.jiec.2013.11.005.
[24] X. Zeng, X. Xiao, J. Chen, H. Wang, Electron-hole interactions in choline-phosphotungstic acid boosting molecular oxygen activation for fuel desulfurization, Appl. Catal., B 248 (2019) 573–586, https://doi.org/10.1016/j.apcatb.2018.09.038.
[25] X. Zeng, X. Xiao, Y. Li, J. Chen, H. Wang, Deep desulfurization of liquid fuels with molecular oxygen through graphene photocatalytic oxidation, Appl. Catal., B 209 (2017) 98–109, https://doi.org/10.1016/j.apcatb.2017.02.077.
[26] W. Zhang, H. Zhang, J. Xiao, Z. Zhao, M. Yu, Z. Li, Carbon nanotube catalysts for oxidative desulfurization of a model diesel fuel using molecular oxygen, Green Chem 16 (2014) 211–220, https://doi.org/10.1039/C3GC41106K.
[27] H. Yang, Q. Zhang, J. Zhang, L. Yang, Z. Ma, L. Wang, H. Li, L. Bai, D. Wei, W. Wang, H. Chen, Cellulose nanocrystal shelled with poly(ionic liquid)/polyoxometalate hybrid as efficient catalyst for aerobic oxidative desulfurization, J. Colloid Interface Sci. 554 (2019) 572–579, https://doi.org/10.1016/j.jcis.2019.07.036.
[28] Y. Wu, P. Wu, Y. Chao, J. He, H. Li, L. Lu, W. Jiang, B. Zhang, H. Li, W. Zhu, Gas-exfoliated porous monolayer boron nitride for enhanced aerobic oxidative desulfurization performance, Nanotechnology 29 (2017), 025604, https://doi.org/10.1088/1361-6528/aa9bc7.
[29] P. Wu, Y. Wu, L. Chen, J. He, M. Hua, F. Zhu, X. Chu, J. Xiong, M. He, W. Zhu, H. Li, Boosting aerobic oxidative desulfurization performance in fuel oil via strong metal-edge interactions between Pt and h-BN, Chem. Eng. J. 380 (2020), 122526, https://doi.org/10.1016/j.cej.2019.122526.
[30] I. Shafiq, S. Shafique, P. Akhter, M. Ishaq, W. Yang, M. Hussain, Recent breakthroughs in deep aerobic oxidative desulfurization of petroleum refinery products, J. Clean. Prod. 294 (2021), 125731, https://doi.org/10.1016/j.jclepro.2020.125731.
[31] X. Zhou, J. Li, X. Wang, K. Jin, W. Ma, Oxidative desulfurization of dibenzothiophene based on molecular oxygen and iron phthalocyanine, Fuel Process. Technol. 90 (2009) 317–323, https://doi.org/10.1016/j.fuproc.2008.09.002.

[32] S. Chen, W. Lu, Y. Yao, H. Chen, W. Chen, Oxidative desulfurization of dibenzothiophene with molecular oxygen catalyzed by carbon fiber-supported iron phthalocyanine, React. Kinet. Mech. Catal. 111 (2014) 535–547, https://doi.org/10.1007/s11144-013-0661-3.
[33] T. Buck, H. Bohlen, D. Wöhrle, G. Schulz-Ekloff, A. Andreev, Influence of substituents and ligands of various cobalt (II) porphyrin derivatives coordinately bonded to silica on the oxidation of mercaptan, J. Mol. Catal. 80 (1993) 253–267, https://doi.org/10.1016/0304-5102(93)85082-5.
[34] Y. Shi, G. Liu, B. Zhang, X. Zhang, Oxidation of refractory sulfur compounds with molecular oxygen over a Ce–Mo–O catalyst, Green Chem 18 (2016) 5273–5279, https://doi.org/10.1039/C6GC01357K.
[35] S.A. Yashnik, A.V. Salnikov, M.A. Kerzhentsev, A.A. Saraev, V.V. Kaichev, L. M. Khitsova, Z.R. Ismagilov, J. Yamin, O.R. Koseoglu, Effect of the nature of sulfur compounds on their reactivity in the oxidative desulfurization of hydrocarbon fuels with oxygen over a modified CuZnAlO catalyst, Kinet. Catal. 58 (2017) 58–72, https://doi.org/10.1134/S0023158417010128.
[36] H. Lu, Y. Zhang, Z. Jiang, C. Li, Aerobic oxidative desulfurization of benzothiophene, dibenzothiophene and 4,6-dimethyldibenzothiophene using an Anderson-type catalyst $[(C_{18}H_{37})_2N(CH_3)_2]_5[IMo_6O_{24}]$, Green Chem 12 (2010) 1954–1958, https://doi.org/10.1039/C0GC00271B.
[37] H. Lü, W. Ren, W. Liao, W. Chen, Y. Li, Z. Suo, Aerobic oxidative desulfurization of model diesel using a B-type Anderson catalyst $[(C_{18}H_{37})_2N(CH_3)_2]_3Co(OH)_6Mo_6O_{18}\bullet 3H_2O$, Appl. Catal., B 138 (2013) 79–83, https://doi.org/10.1016/j.apcatb.2013.02.034.
[38] E. Eseva, A. Akopyan, A. Schepina, A. Anisimov, A. Maximov, Deep aerobic oxidative desulfurization of model fuel by Anderson-type polyoxometalate catalysts, Cat. Comm. 149 (2021), 106256, https://doi.org/10.1016/j.catcom.2020.106256.
[39] J. Yu, Z. Zhu, Q. Ding, Y. Zhang, X. Wu, L. Sun, J. Du, Oxidative desulfurization of dibenzothiophene with molecular oxygen using cobalt and copper salen complexes encapsulated in NaY zeolite, Catal. Today 339 (2002) 105–112, https://doi.org/10.1016/j.cattod.2019.05.053.
[40] H.-.X. Yuan, Q.-.H. Xia, H.-.J. Zhan, X.-.H. Lu, K.-.X. Su, Catalytic oxidation of cyclohexane to cyclohexanone and cyclohexanol by oxygen in a solvent-free system over metal-containing ZSM-5 catalysts, Appl. Catal., A 304 (2006) 178–184, https://doi.org/10.1016/j.apcata.2006.02.037.
[41] J. Liu, C. Peng, X. Shi, Preparation, characterization, and applications of Fe-based catalysts in advanced oxidation processes for organics removal: a review, Environ. Pollut. 293 (2022), 118565, https://doi.org/10.1016/j.envpol.2021.118565.
[42] H. Du, F. Deng, R.R. Kommalapati, A.S. Amarasekara, Iron based catalysts in biomass processing, Renew. Sust. Energ. Rev. 134 (2020), 110292, https://doi.org/10.1016/j.rser.2020.110292.
[43] Z. Gholami, F. Gholami, Z. Tišler, J. Hubáček, M. Tomas, M. Bačiak, M. Vakili, Production of light olefins via Fischer-Tropsch process using iron-based catalysts: a review, Catalysts 12 (2022) 174, https://doi.org/10.3390/catal12020174.
[44] N. Nagarjun, A. Dhakshinamoorthy, Aerobic oxidation of benzylic hydrocarbons by iron-based metal organic framework as solid heterogeneous catalyst, Chem. Select 3 (2018) 12155–12162, https://doi.org/10.1002/slct.201802672.
[45] C. Parmeggiani, F. Cardona, Transition metal based catalysts in the aerobic oxidation of alcohols, Green Chem 14 (2012) 547–564, https://doi.org/10.1039/C2GC16344F.
[46] D.E. Tsaplin, D.A. Makeeva, L.A. Kulikov, A.L. Maksimov, E.A. Karakhanov, Synthesis of ZSM-12 zeolites with new templates based on salts of ethanolamines, Russ. J. Appl. Chem. 91 (2018) 1956–1961, https://doi.org/10.1134/S1070427218120066.
[47] D.E. Tsaplin, E.R. Naranov, L.A. Kulikov, I.S. Levin, S.V. Egazar'yants, A. L. Maksimov, E.A. Karakhanov, Crystallization of zeolites in the presence of diquaternary alkylammonium salts derived from dimethylethanolamine, Pet. Chem. 61 (2021) 815–824, https://doi.org/10.1134/S0965544121080089.
[48] L.A. Kulikov, D.E. Tsaplin, M.I. Knyazeva, I.S. Levin, S.V. Kardashev, T. Y. Filippova, A.L. Maksimov, E.A. Karakhanov, Effect of template structure on the zeolite ZSM-12 crystallization process characteristics, Pet. Chem. 59 (2019) 60–65, https://doi.org/10.1134/S0965544119130097.
[49] Q. Tang, H. Xu, Y. Zheng, J. Wang, H. Li, J. Zhang, Catalytic dehydration of methanol to dimethyl ether over micro–mesoporous ZSM-5/MCM-41 composite molecular sieves, Appl. Catal., A 413-414 (2012) 36–42, https://doi.org/10.1016/j.apcata.2011.10.039.
[50] N. Jaafar, A. Abdul Jalil, S. Triwahyono, M. Muhd Muhid, N. Sapawe, M. Satar, H. Asaari, Photodecolorization of methyl orange over α-Fe_2O_3-supported HY catalysts: the effects of catalyst preparation and dealumination, Chem. Eng. J. 191 (2012) 112–122, https://doi.org/10.1016/j.cej.2012.02.077.
[51] Y. Kamimura, K. Iyoki, S.P. Elangovan, K. Itabashi, A. Shimojima, T. Okubo, OSDA-free synthesis of MTW-type zeolite from sodium aluminosilicate gels with zeolite beta seeds, Microporous Mesoporous Mater 163 (2012) 282–290, https://doi.org/10.1016/j.micromeso.2012.07.014.
[52] A.S. Araujo, Catalytic properties of HZSM-12 zeolite in the n-heptane catalytic cracking, React. Kinet. Catal. Lett. 84 (2005) 287–293, https://doi.org/10.1007/s11144-005-0221-6.
[53] A.S. Araujo, A.O.S. Silva, M.J.B. Souza, A.C.S.L.S. Coutinho, J.M.F.B. Aquino, J. A. Moura, A.M.G. Pedrosa, Crystallization of ZSM-12 zeolite with different Si/Al ratio, Adsorption 11 (2005) 159–165, https://doi.org/10.1007/s10450-005-4909-8.
[54] Q. Liu, D. Wen, Y. Yang, Z. Fei, Z. Zhang, X. Chen, J. Tang, M. Cui, X. Qiao, Enhanced catalytic performance for light-olefins production from chloromethane over hierarchical porous ZSM-5 zeolite synthesized by a growth-inhibition strategy, Appl. Surf. Sci. 435 (2018) 945–952, https://doi.org/10.1016/j.apsusc.2017.11.153.
[55] B.H. Chiche, R. Dutartre, F. Renzo, F. Fajula, A. Katovic, A. Regina, G. Giordano, Study of the sorption and acidic properties of MTW-type zeolite, Catal. Lett. 31 (1995) 359–366, https://doi.org/10.1007/BF00808600.
[56] J. Li, P. Miao, Z. Li, T. He, D. Han, J. Wu, Z. Wang, J. Wu, Hydrothermal synthesis of nanocrystalline H[Fe, Al]ZSM-5 zeolites for conversion of methanol to gasoline, Energy Convers. Manag. 93 (2015) 259–266, https://doi.org/10.1016/j.enconman.2015.01.031.
[57] K. Wang, M. Dong, X. Niu, J. Li, Z. Qin, W. Fan, J. Wang, Highly active and stable Zn/ZSM-5 zeolite catalyst for the conversion of methanol to aromatics: effect of support morphology, Catal. Sci. Technol. 8 (2018) 5646–5656, https://doi.org/10.1039/C8CY01734D.
[58] S. Ivanova, C. Lebrun, E. Vanhaecke, C. Pham-Huu, B. Louis, Influence of the zeolite synthesis route on its catalytic properties in the methanol to olefin reaction, J. Catal. 265 (2009) 1–7, https://doi.org/10.1016/j.jcat.2009.03.016.
[59] M. Shi, D. Zhang, X. Yu, Y. Li, X. Wang, W. Yang, Deep oxidative desulfurization catalyzed by $(NH_4)_5H_6PV_8Mo_4O_{40}$ using molecular oxygen as an oxidant, Fuel Process. Technol. 160 (2017) 136–142, https://doi.org/10.1016/j.fuproc.2017.02.038.
[60] E.M. Rodríguez, G. Márquez, M. Tena, P.M. Álvarez, F.J. Beltrán, Determination of main species involved in the first steps of TiO_2 photocatalytic degradation of organics with the use of scavengers: the case of ofloxacin, Appl. Catal., B 178 (2015) 44–53, https://doi.org/10.1016/j.apcatb.2014.11.002.
[61] E. Karakhanov, A. Akopyan, O. Golubev, A. Anisimov, A. Glotov, A. Vutolkina, A. Maximov, Alkali earth catalysts based on mesoporous MCM-41 and Al-SBA-15 for sulfone removal from middle distillates, ACS Omega 4 (2019) 12736–12744, https://doi.org/10.1021/acsomega.9b01819.